RESEARCH

Testing of a new Yb:YAG fiber laser system for the removal of graphic vandalism from marble

Amelia Suzuki[1], Cristiano Riminesi[1], Marilena Ricci[2], Silvia Vettori[1] and Barbara Salvadori[1*]

Abstract

Graphic vandalism causes detrimental effects on architectural stone surfaces. Among the cleaning methods developed in the last decades, laser cleaning showed considerable effectiveness but the available equipment still lacks full adaptability for the use on site, while the cleaning process is time-consuming for the site work requirements. In this paper, the feasibility of a fiber laser operating at 1064 nm (Yb:YAG) at high repetition rate (kHz) for the removal of vandal graffiti from marble is investigated, as it is potentially suitable for cleaning of large surfaces. Indeed, this device exploits a scan system covering a wider area than that of solid state lasers, while maintaining excellent portability. Evaluation of the cleaning procedure on a selection of spray paints and felt-tip permanent markers applied on marble mock-ups is carried out with a multimodal approach (optical microscopy combined with surface pattern reconstruction, colour monitoring, Fourier Transform Infrared spectroscopy in external reflection and ATR mode, Thin Layer Chromatography, Raman spectroscopy, thermal monitoring, scanning electron microscopy). Ablation and thermal effects are observed varying the laser setting and the type of paint layer, with repetition rate showing a strong impact on the type of interaction. Overall, best cleaning procedures are achieved for the thinning of the black marker and the removal of the black spray paint. Some residues on the best results were observed, suggesting that the laser needs to be integrated with a second step of chemical cleaning. This study, focused on graffiti removal, shows that fiber laser can be a useful tool for cleaning of large monumental surfaces.

Keywords Graffiti removal, Laser cleaning, Yb-doped fiber laser, Spray paint, Marker pen
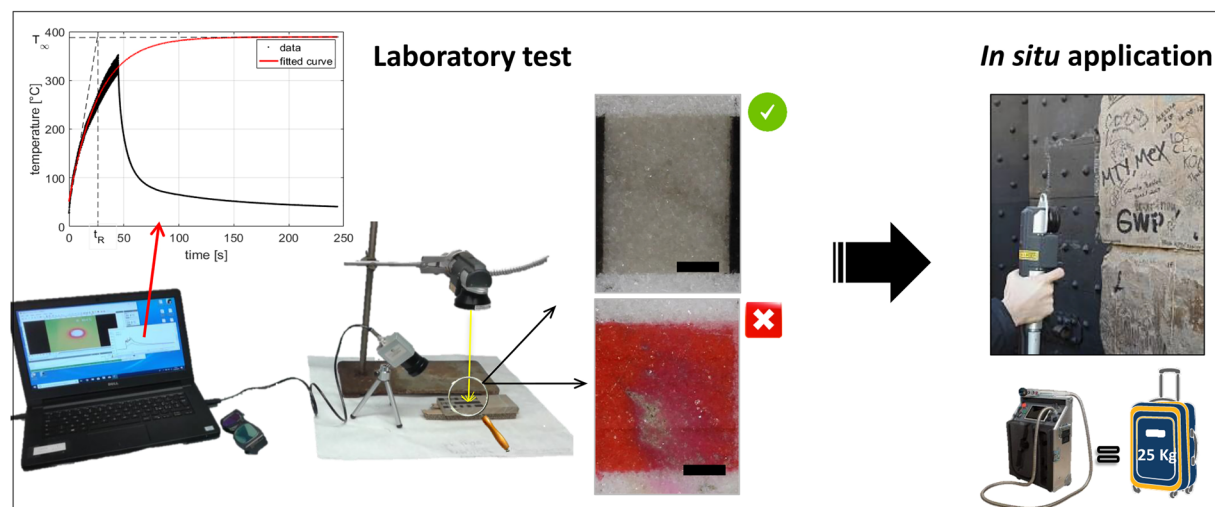
*Correspondence:
Barbara Salvadori
barbara.salvadori@cnr.it
Full list of author information is available at the end of the article

Graphical Abstract

Introduction

Graphic vandalism poses a risk for the conservation of Architectural Heritage as it can accelerate stone decay leading to considerable loss in value and significance. Many specific cleaning methods have been studied in the last decades and thoroughly described by reviews [1–3], as well as anti-graffiti coatings have been investigated [4–6]. Among the traditional procedures adopted to remove undesired paint layers, mechanical methods (e.g., water jet technology [7, 8], grit-blasting [9, 10]) and chemical products (organic solvents or alkali caustic removers [7, 9, 11]) are commonly used. These methods are potentially harmful causing detrimental effects to the substrates such as abrasion of the surfaces [12] or in-depth paint migration [13]. Promising advances with some innovative materials (silica sol–gel [14], hydrogels [15] or nanostructured fluids [16]) have been done in recent years on chemical cleaning front, however further work is still needed to fully understand the interaction with stone and paint, as well as the permanence of chemical residues. In the last decades, the use of lasers has been widely investigated: more than half of the consulted studies in a recent review [1] are centered on the use of laser for graffiti removal, which is an interesting alternative to more conventional cleaning methods. The most used lasers in stone cleaning are the different harmonics-wavelengths of neodymium-based systems, i.e., Nd:YAG or Nd:YVO$_4$ [1, 9, 17]. Laser cleaning provides an effective solution for the removal of graffiti made of spray varnishes [17–21] and permanent markers [22], but such technique does not seem fully adaptable to the requirements of portability and handling necessary for site works and compatible with cleaning interventions on large surfaces.

Recently, also the combination of laser and chemical action has been proved successful by some authors [23–25].

The advantages of laser approach over conventional methods are non-mechanical contact, selectivity and the possibility to adjust the cleaning conditions in real time. Indeed, one of the interesting practical aspects of the use of lasers is the possibility of tuning the settings to obtain the desired cleaning levels. While performing laser cleaning, if the thickness and consistency of the layer to be removed change, it is possible to blur the laser beam by changing the working distance; this permits amplification of the beam size and reduction of the fluence, which results in a lighter cleaning effect. Nevertheless, the small size of the laser beam spot (usually less than 1–2 mm^2), in solid state laser systems currently used for this purpose, makes the cleaning operations slow and time consuming, with a non-negligible economic impact that should be considered in terms of benefit–cost ratio [12], especially when this method is applied to large surfaces such as those where vandals often act with spray paints. Moreover, solid-state laser systems such as Nd:YAG and Nd:YVO$_4$ are generally heavy and cumbersome, as well as sensitive to mechanical stress (due to eventual misalignment of the optics) which make their handling and use on scaffolds difficult. The laser-material interaction studies when performing cleaning of artworks were mainly focused on understanding the influence of wavelength,

Suzuki *et al. Heritage Science*   (2023) 11:132

Page 3 of 20

pulse duration and fluence [26–28], while the effect of the repetition rate on the ablation efficiency has not been extensively investigated in the field of laser cleaning of artworks, due to the limited range of repetition frequency (generally 1–10 Hz). Only few studies were performed for Q-switched second harmonic of Nd:YAG and UV Nd:YVO$_4$ up to 10 kHz [29, 30] and with picosecond lasers [31].

Without detracting from the proven validity of flash lamped solid-state systems in surface cleaning, it is worth considering alternative solutions that can be useful in situations where rapidity of action and handling are essential. In this context, interesting devices are the Yb-doped fiber laser systems [32, 33], recently made available on the market. Such instruments are easily transportable even on scaffolding thanks to their compactness and lightness, and they require relatively limited maintenance. These fiber lasers can operate at high repetition rate (over 1 kHz) with a beam scan system. Despite the features of the Yb:YAG laser systems that make them attractive for applications in the field of heritage conservation, only a couple of studies have been reported for the qualitative evaluation of deposits removal from stone with similar devices [34, 35]. To our knowledge, although they have been used in some public demonstrations [36], no systematic studies have been carried out to evaluate their effectiveness and harmfulness for stone cleaning [37]. However, in the field of material processing, Cu-based alloys cleaning was recently performed assessing the driving mechanisms by ToF–SIMS spectroscopy [38].

In this work, we aim to explore the feasibility of a 1064 nm Q-Switched Yb:YAG fiber laser for the cleaning of graffiti from marble. To assess the impact of these systems on the ablation mechanism, a systematic evaluation is required. In our research, the evaluation of treatment's effectiveness of Yb:YAG fiber laser was performed focusing the attention on: (1) the residual of paint after the laser treatment and (2) the effects of the laser radiation induced on the surface. The outcome is demonstrated on the thinning or removal of two colours (red and black) of Montana Colours alkyd-based spray paints and of Tratto FILA permanent markers, representative of the most diffused types of vandal acts on stone artworks. Different laser parameters were tested evaluating the cleaning efficacy and checking the harmfulness to the substrate. Colorimetric analyses, photographic documentation, ER-FTIR were used to compare the surface chromatic evolution and ascertain the presence of remnants. The efficiency and invasiveness of the Yb:YAG laser cleaning on marble was evaluated by monitoring the morphology and roughness variations at the optical microscope, exploiting 3D reconstruction of surface pattern as well. Micro-Raman was also used on Thin Layer Chromatography (TLC) to investigate the composition of the two permanent markers. Finally, since the determination of thermal state of the surface in the irradiated area may allow to correlate the physical and chemical processes that take place, thermal monitoring of the surfaces during the treatments was performed to help understand the specific laser-material interaction mechanisms of this new laser system, which is essential in the perspective of damage risk reduction.

Materials and methods
Samples preparation
The cleaning tests were carried out on a traditional lithotype used in architecture, Carrara marble [39, 40], with the aim of thinning a simulated graffiti made of:

a. Two low pressure spray paints whose colours were identified by their RAL codes [41] (MNT94 MontanaColours® [42] RV-9011 Matt black, MB and RV-241 Madrid red, MR) [23, 30, 43].
b. Two felt-tip permanent markers by Tratto FILA, colours black (FB) and red (FR) [44–46].

These two types of paint were chosen for their popular use in graphic vandalism and for their different chemical composition and rheological behaviour; spray paints have a high percentage of binder which creates a quite elastic, thick paint layer on the surfaces, while the permanent markers are more liquid due to a higher solvent content and penetrate more in the porosity of the stone, creating a very thin paint layer. In addition, at 1064 nm the MB presents low reflectance, while FB and the two reds (MR and FR) display high reflectance [30, 46].

Four Carrara marble samples ($10 \times 10 \times 1$ cm^3) were polished with 120-grit sandpaper, washed with deionized water and air-dried for one week. The composition and microstructure of the marble were reported elsewhere [47] and consisted mainly of calcite with traces of dolomite, mica, oxides and pyrite in the veins. The microfabric ranged from granoblastic to heteroblastic, with predominantly straight grain boundaries. Mean grain size ranged from 150 to 200 μm; crystal shape varied from euhedral to subhedral. The total open porosity was 2.8% while the effective porosity (accessible to water) was 1.1%. Pore size distribution was unimodal, with average pore radius 0.084 μm measured by mercury porosimeter in previous investigation [48].

On each sample, three stripes (10×1 cm^2) were coloured with the different paints selected, keeping as many application parameters as possible constant, to provide homogeneous and similar paint thickness on all the samples. For spray paints, the samples were sprayed once with the same application distance (30 cm), inclination

Suzuki *et al. Heritage Science*   (2023) 11:132

Page 4 of 20

(angle 90°) and spraying time (2 s). For markers, only one coat was applied keeping the same pressure of the tip on the surface. The samples were left to air-dry in the laboratory (20 ± 2 °C; $60\pm10\%$ RH) for one month before characterization, which was considered as a suitable time for complete drying according to the technical sheet [49]. Figure 1 shows the morphology and thickness of the paints in cross section, which is different depending on the type and colour: 5–15 µm for FB and FR, 60–80 µm for MB and 40–50 µm for MR. The cleaning tests were performed 1 month after the preparation of mock-ups.

### Instruments and methods for the characterization of paints

The paints were spread with felt-tip pen or sprayed on glass slides and scraped off after drying, in order to be characterized with a multi-analytical approach. The elemental composition of the paints was analysed with an X-ray fluorescence spectrometer, XRF (handheld TraCer III-SD spectrometer by Bruker). The instrument is equipped with a Rhodium X-ray tube and an SDD detector. Spectra were recorded with an aluminium and titanium filter to empathize Ti to Ag, W to Bi, at 40 kV and current 12 µA, acquisition time 60 s, using the S1PXRF dedicated software. The main binders present in the selected permanent markers and spray paints were characterized with a portable Alpha Bruker FT-IR spectrometer, equipped with an ATR diamond in the range 4000–400 cm^{-1}, 24 scans, resolution 4 cm^{-1}. The spectra were processed with OPUS 7.2 software.

Further attempts to identify the dyestuffs present in the markers were performed by analytical TLC separation, which gave an overview of the complexity of the dyes' mixtures. The inks were directly applied on pre-coated glass plates with 0.15–0.2 mm-thick silica gel (HPTLC pre-coated silica gel 60 glass plates, Merck, Germany) and eluted in a glass chamber using a basic eluent commonly used for inks chromatography with complex dyes mixtures [44, 45, 50], iso-BuOH:EtOH:NH$_3$ (7.6 M) with a ratio of 5:2:3 (w/w). The separated spots were visualized clearly and they were analysed directly on the TLC plate by micro-Raman spectroscopy, by means of a Renishaw RM2000 single grating (1200 g/mm) spectrometer equipped with a Peltier-cooled CCD detector at − 20 °C. A near infrared diode laser (785 nm) was employed as excitation source. Spectra were acquired using a 50x (N.A.=0.75) magnification objective, providing a spatial resolution of about 2 µm. The investigated spectral range was between 200 and 1800 cm^{-1} and 3400–3700 cm^{-1} with a spectral resolution of 4 cm^{-1}. Acquisition times were on the order of 30 s and the laser power on the order of a few mW on the samples. The spectrometer was calibrated with respect to the 520 cm^{-1} band of a silicon wafer.

Characterization of paints

FTIR spectra of FB and FR show the main absorptions of styrene (Sty) as three very weak bands between 3083 and 3026 cm^{-1} and two bands at 2930 and 2872 cm^{-1} due to the C−H stretching vibrations; absorptions at 1452 and
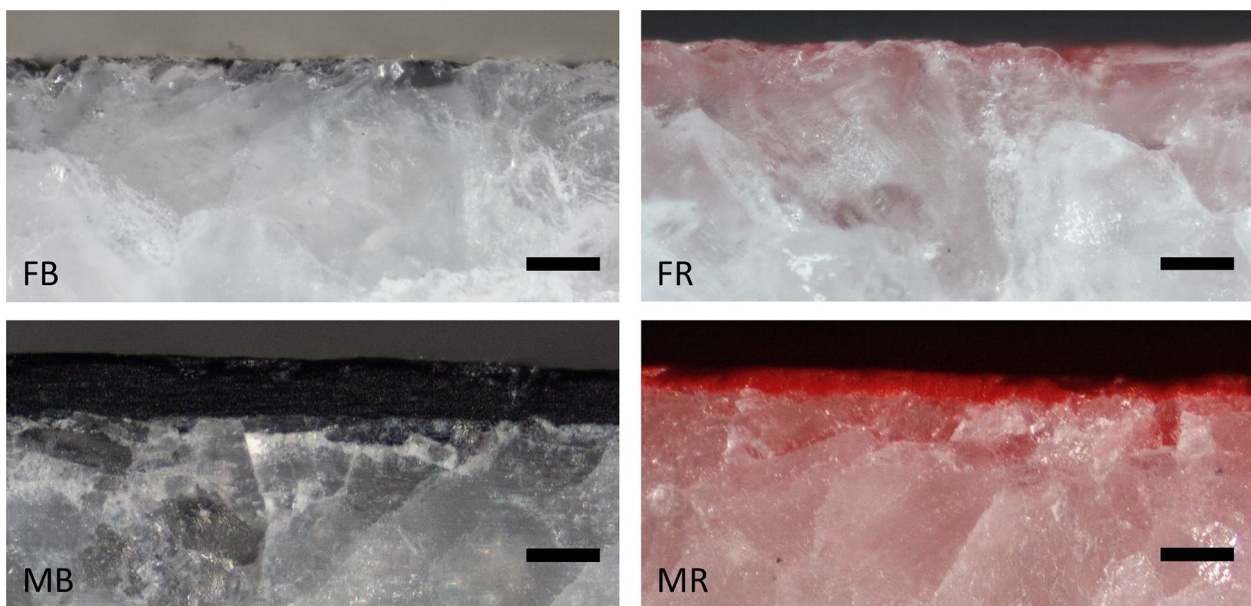
Fig. 1 Optical microscope observation of cross sections of black (FB) and red (FR) felt-tip pens and of black (MB) and red (MR) spray paints on marble. Bar: 100 µm

Suzuki *et al. Heritage Science*   (2023) 11:132

Page 5 of 20

1496 cm^{-1}, which can be ascribed to the aromatic skeletal ring breathing vibrations, and aromatic C–H out-of-plane bending modes at 702 and 754 cm^{-1} [43]. In FR, the spectral profile also included a complex suite of bands in the 1800–700 cm^{-1} region which suggested the presence of a Rhodamine-type dye. The peak at 2974 cm^{-1} was assigned to the C–H stretching mode, while the mode corresponding to the 1718 cm^{-1} IR band was assigned to the C=O bond stretching of the external carbonyl group. The strong band at 1600 cm^{-1} was due to the C–C skeletal stretching vibration of the external phenyl ring. Ethylamino groups deformations occurred between 1421 and 1452 cm^{-1}, while C–H bending of the external groups appeared as a strong band at 1307 cm^{-1}. The vibrations at 1269 and 1246 cm^{-1} were due to external C–O stretching and C–O–C stretching modes, respectively [51].

In FB, the presence of methyl violet was hypothesized, due to vibration bands attributable to triphenylmethane as well as to the colour of the eluted fraction on TLC (vide infra). The C=C stretching vibration of the benzene ring was detected at 1586 cm^{-1}, while the band at 1362 and 1171 cm^{-1} correspond to the CH$_3$ methyl rocking and to the aromatic C-N stretching vibrations, respectively [52].

TLC separation allowed to highlight the presence of two different dyes in the red ink of FR: one magenta and one yellow (Fig. 2). The micro-Raman analysis of the magenta spot (Fig. 2a) confirmed the presence of

Rhodamine 6G, as results by the comparison with the literature [53]. The identification of the yellow dye was made difficult by the high fluorescence of the background and the low concentration. Some characteristic Raman bands attributed to main chemical groups are present (Fig. 2b); however, spectrum lacks information in comparison to standard dyes. The pattern of Raman signals can be related to fluorescent yellow azo-dyes that give rise to strong Raman bands in the range 1400–1600 cm^{-1}, due to the N=N stretching vibrations and mainly aromatic C=C stretching in the phenyl ring; in addition, the aromatic ring vibrations are visible at 1000, 755 and 643 cm^{-1}. The strong 1150 cm^{-1} vibration can be attributed to the C–N (azo) symmetric stretching mode.

In FB, the ink was separated in a black spot that was not eluted, suggesting the presence of carbon black (Additional file 1: Fig. S1), and a violet-bluish spot compatible with triarylmethane dyes, methyl violet suggested by FTIR analyses. The micro-Raman spectra obtained in the bluish spot (Fig. 2c) show bands very similar to 1587, 1566, and 1452 cm^{-1}, which are associated to the stretching of the benzene rings and the bending vibration of CH$_3$, respectively in the triarylmethane compounds and 1330, 817 and 750 cm^{-1} bands associated to CCC asymmetric stretching, bending of (CH)$_{ring}$, and both CCC symmetric stretching and CN bond stretching, respectively. On the contrary, it is not possible to unambiguously assign all peaks given by the blue fraction, most
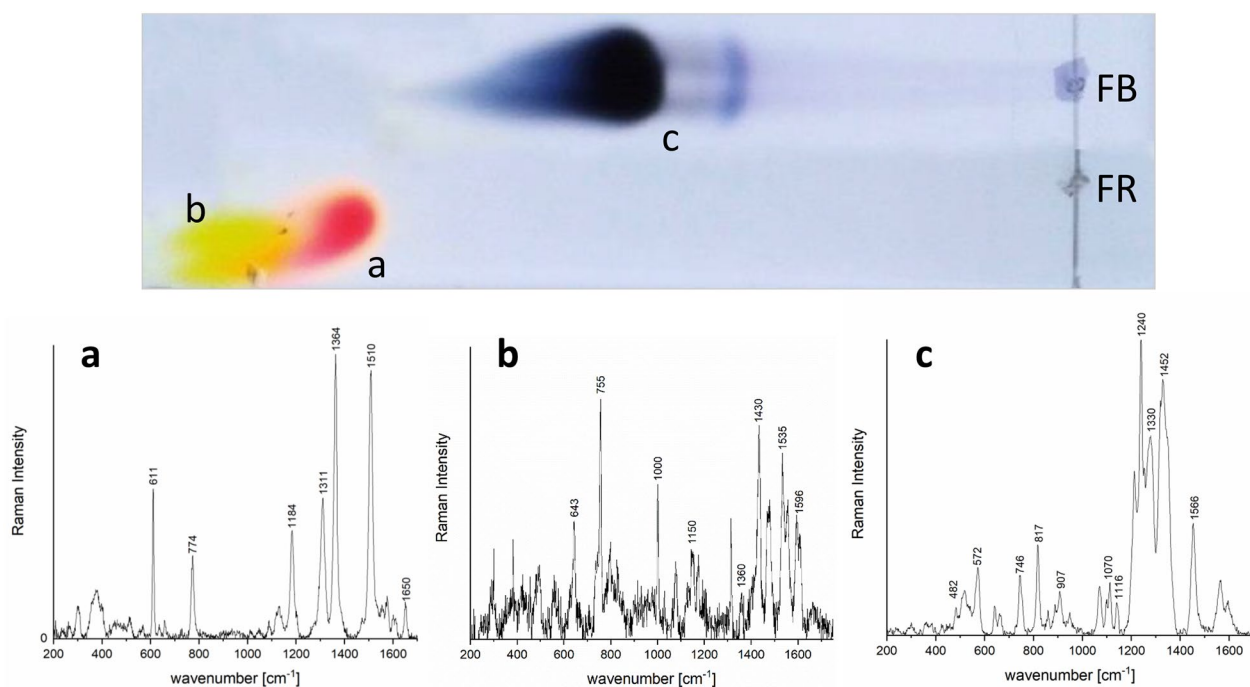
Fig. 2 Raman spectra of TLC eluted fractions: **a** magenta; **b** yellow; **c** violet-bluish

likely due to the presence of other components eluting together with the violet-bluish dye. The use of these dyes, combined with amorphous carbon, is common in the production of inks, as the triarylmethane compounds are quite opaque and with improved colour stability [54].

XRF detected the presence of chrome (Cr) in FB (data not shown), suggesting the presence of aniline black that, however, was not confirmed by FTIR and Raman analyses.

For the selected spray paints, the presence of an alkyd resin in MB and of alkyd-amino resin in the MR, as binding media, was assessed with different analytical techniques in a previous work [23] and further confirmed by FTIR analyses, where the typical spectral pattern of alkyd resins was clear (Additional file 1: Fig. S2) [55]. The C-H asymmetric and symmetric stretching vibrations were found at 2925 and 2855 cm^{-1}, respectively, as well as the strong C=O stretching at 1726 cm^{-1}. In the fingerprint region, the weak doublet at 1600 and 1580 cm^{-1} was attributed to the aromatic ring stretching vibration, while C–H bending (1450 cm^{-1}), C–C and C–C stretching bands were detected at 1258 and 1120 cm^{-1}, respectively. The peak at 1070 cm^{-1} corresponded to unsaturated aromatic in-plane deformation, while 741 and 705 cm^{-1} bands were attributed to aromatic out-of-plane bending of the polyester portion of the resin.

XRF analyses detected titanium (Ti) in MR, suggesting the presence of rutile, and calcium (Ca) in all the paints (spectra not shown), ascribable to the presence of chalk as an extender.

Cleaning tests
INFINITO system
The laser used in this research is a NIR Q-switched Yb:YAG (mod. INFINITO 50 W by El.En. SpA), emitting at 1064 nm with pulse duration of 100 ns exploiting variable spot sizes varying the available lens. A brief summary on the characteristics and operational modes of the INFINITO system are displayed in Table 1 (further information can be found in [56]).

The main features are the working frequency in kHz and a scanning system that allows to treat areas up to 40×20 mm^2. The area can be scanned line by line, or with circle or by brush mode (Fig. 3). In particular, the brush mode is characterized by four specific parameters: scan speed, scan size, brush width and brush fill. This mode consists of a simultaneous scan of the beam through the X and Y directions, creating a rectangular irradiation area (Fig. 3). The size of the area is defined by the scan size parameter—along the X or Y direction—and by the brush width that is the half of the scan size. The brush fill is the interlining, and in combination with the repetition frequency defines the effective irradiated surface within

Table 1 Summary of INFINITO system specifications

|	
Average power (P_N) [W]	50
Dimension [cm]	$63 \times 45 \times 26$
Weight [kg]	25
Lens [mm]	250; 355; 500
Fluence [J/cm^2]	2–20
Repetition frequency [kHz]	20–200
Spot size [µm]	80; 110; 160
Scan modes	Line, circle and brush
Scan size [mm]	5–80
Brush width [mm]	2.5–40
Brush fill [mm]	0.1–0.9

the selected scanned area. The brush mode is particularly useful to ensure reproducibility of cleaning on the test areas because it allows maintaining the same setting during the treatment. Indeed, the hand piece is fixed at an established distance from the surface, thus avoiding the variability introduced by the movement of the handle by the operator or the necessity to use x–y stages to move the samples. This is different from lamp pumped solid-state lasers operating in Hz, where the movement of the handle may modify the fluence applied not guaranteeing homogeneous cleaning of the treated area. For this reason, all the tests were performed with the brush mode.

All the cleaning tests were made under fume hood at room temperature and with the handle positioned normal to the surface to be cleaned.

Preliminary tests performed on a marble mock-up painted with MB allowed to select spot size, scan speed and brush setting. The 110 µm spot size was chosen as it is intermediate among the available ones, exploiting a maximum fluence of about 10 J/cm^2. Varying the frequency and scan speed allowed to observe and estimate the spot overlap as shown in the graph of Fig. 4. At a fixed scan speed, the laser spot overlap increases with the frequency. So, performing laser cleaning in kHz regime creates a condition in which the laser radiation dose (energy per unit of time, that is the peak power) on a single spot is not defined by the single fluence per pulse as the energy contribution on each spot is affected from the previous and the following laser pulse due to the overlapping. Moreover, brush size, width and fill were varied to define the best brush setting for homogeneous cleaning tests. Within the irradiated area the wider the fill (max BF is 0.9 mm) the less homogenous the cleaning effect, since some parts of the scan area were not irradiated, as shown in the stereomicroscope image in Fig. 4. The non-irradiated parts are located among the edges of the width side due to the shape of the scan and appear when consecutive spots do not overlap.

Suzuki *et al. Heritage Science*   (2023) 11:132

Page 7 of 20
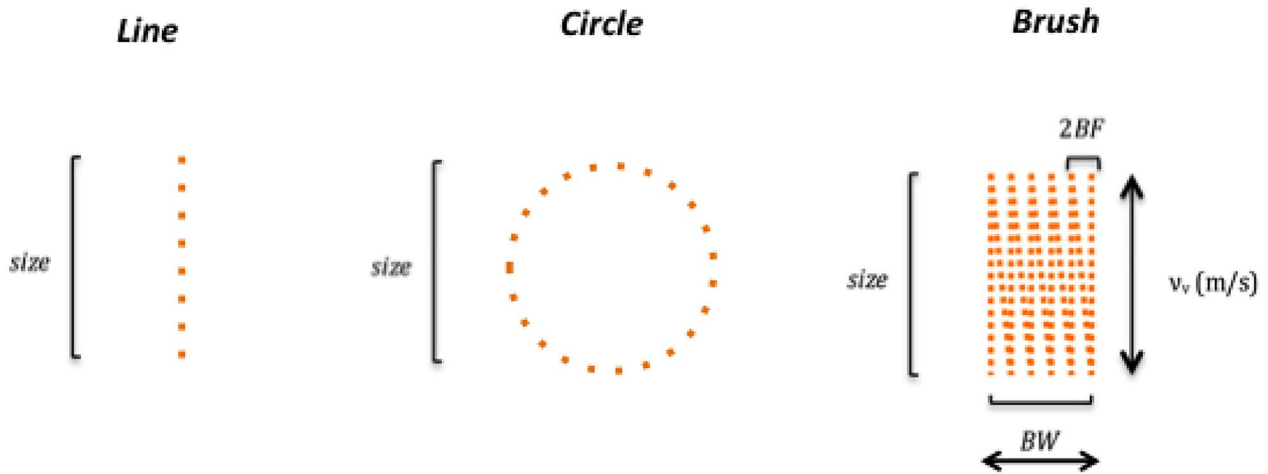
Fig. 3 The three scan modalities of the Yb:YAG fiber laser, INFINITO. BF is the brush fill and BW is the brush width
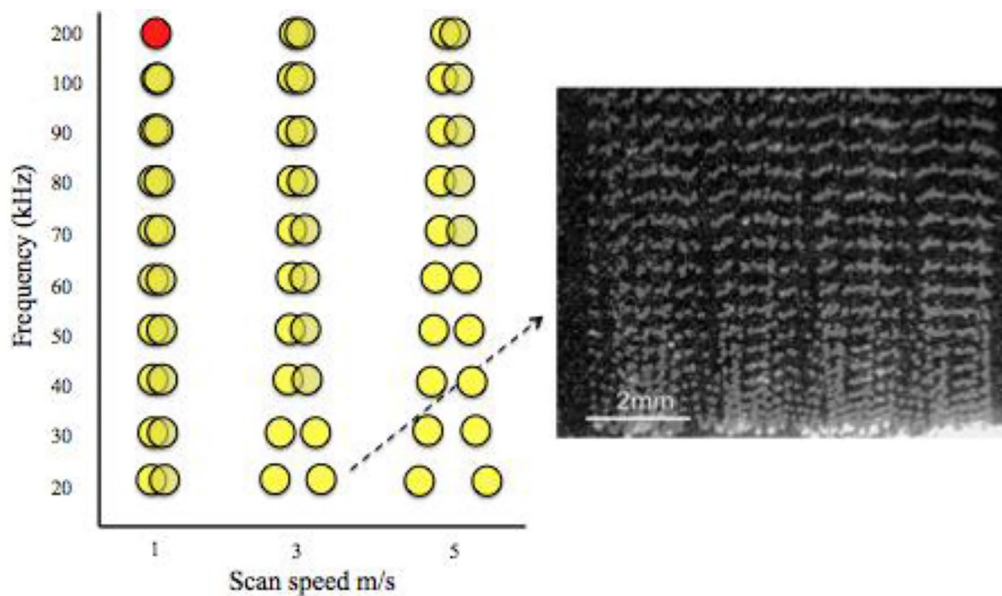
Fig. 4 Graphic representation of two consecutive laser pulses with different combinations of frequency and scan speed. On the right, stereomicroscope image showing the effects of few scans on a black spray paint marble mock-up with 20 kHz at the scan speed of 3 m/s, with a scan size of 15 mm and maximum fill (BF = 0.9 mm)

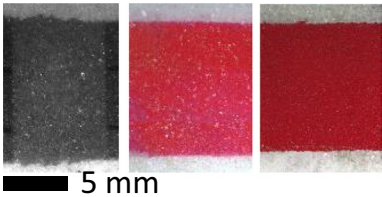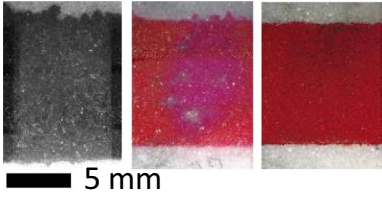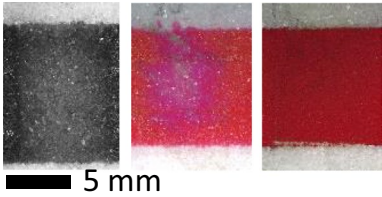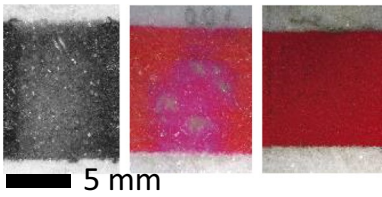Based on the results of preliminary tests, the following settings have been selected:
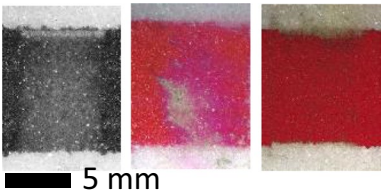
– Average power $(P_N) \geq 40$ W for FB, FR and MR since below this value no removal efficacy was observed, even when the other parameters were varied. Instead, for MB lower P_N values than 40 W were also effective;
– Spot size 110 μm;

– Scan speed fixed at 3 m/s to evaluate the cleaning effects due to the frequency and the overlap;
– The finest BF (0.1 mm), in order to obtain almost parallel line scans within the treated area to favour homogeneity;
– Cleaning areas of 15×7.5 mm^2 (scan size x BW), as it is a suitable dimension for the surface characterization.

Suzuki *et al. Heritage Science*   *(2023) 11:132*

Page 8 of 20

Furthermore, the dry mode was preferred since the water-assisted method, mainly used for black crust removal to minimize the surface heating and to improve the ablation [57], appeared ineffective in this case. This is likely due to the waterproof nature of the graffiti paint that causes the formation of a water layer which mitigates the ablation effect. On the other hand, the solvent-cleaning step is recommended after the main part of the paint has been removed by the laser treatment [23, 24, 58].

The cleaning tests were performed varying the average power (P_N) and the frequency; the correlated peak power (P), pulse energy and fluence are reported. All the cleaning settings performed are listed in Tables 2 and 3 defining a letter for each operative mode used. The irradiation time was kept constant at 40 s for the markers and MR,

Table 2 Summary of the settings of Yb:YAG laser system (INFINITO 50 W by El.En. SpA) used for tests on paint types FB, FR, MR

Operative mode	Laser setting parameters					Visible image of the surface after laser treatment
	P_N [W]	P [kW]	Repetition frequency [kHz]	Energy per pulse [mJ]	Fluence per pulse [J/cm²]	
E	40	10	40	1	10.52	5 mm
F	50	8	60	0.8	8.42	5 mm
G	50	6.3	80	0.63	6.63	5 mm
H	50	5	100	0.5	5.26	5 mm
I	50	7	200	0.25	2.63	5 mm

Constant brush mode setting with: scan speed 3 m/s, BW 7.5 mm BF 0.1 mm. The scan size is 15 mm. The spot is 110 μm

Suzuki *et al. Heritage Science*   (2023) 11:132

Page 9 of 20

Table 3 Summary of the settings of Yb:YAG laser system (INFINITO 50 W by El.En. SpA) used for tests on paint type MB

Operative mode	Laser setting parameters					Visible image of the surface after laser treatment
	P_N [W]	P [kW]	Repetition frequency [kHz]	Energy per pulse [mJ]	Fluence per pulse [J/cm^2]	
M	10	5	20	0.5	5.26	5 mm
N	25	5	50	0.5	5.26	5 mm
O	25	3.1	80	0.3	3.29	5 mm
P	40	5	80	0.5	5.26	5 mm
Q	50	6.3	80	0.6	6.58	5 mm

Constant brush mode setting with: scan speed 3 m/s, BW 7.5 mm BF 0.1 mm. The scan size is 15 mm. The spot is 110 µm

while for MB it varied between 3 and 10 s as the cleaning of this varnish is faster. Moreover, the operative modes for MB (Table 3) were set at lower power and repetition frequency compared to the FB, FR and MR (Table 2) because of the more effective interaction with the laser radiation.

Instruments and methods for cleaning evaluation

The evaluation of the effectiveness of the treatments followed the approach of observing the surfaces with full-field techniques from macro towards micro-observations, allowing to focus the spot investigations on the areas of interest [59]. Subsequently, visual and analytical detection of cleaning effectiveness was correlated with the surface temperature recorded for each test to better interpret the ablative/temperature mechanisms.

Chromatic changes were monitored according to the procedure described in European Standard EN15886 [60] using the CIELAB1976 method, with the standard illuminant D65 and observer 10°. The colour coordinates L*, a*, and b* were recorded on each area before painting (t0), after painting (t1) and after cleaning (t2) using a KONICA-MINOLTA CM2600d spectrophotometer with spectral range 360–740 nm (spot size Ø3 mm). SCI

Suzuki *et al. Heritage Science*   (2023) 11:132

Page 10 of 20

data were collected and three measures were performed on each area, to improve data accuracy. The colour variation ΔE is calculated as described in [60] and as detailed in the Supplementary materials.

The spots were localized using a transparent mask delimiting the measurement area for each specimen, with the hole over the spot exactly fitting the colorimeter probe. The colorimeter was calibrated against a SPEC-TRALON reference before each set of measurements.

Observations of the uncleaned/cleaned surfaces to control the morphology and roughness variations were performed both with a stereomicroscope Stemi 2000c Zeiss (1-4X magnifications) with video camera ACT1, and a Nikon Eclipse E600 optical microscope (4-10-20X magnifications) with NIS elements software. The 3D reconstruction of surface pattern, by NIS-Elements imaging software (using appropriate code [61]), allowed to investigate the thickness removed after each laser treatment and the possible substrate abrasion in terms of roughness variation. The roughness information is summarized by the statistical parameter R_a and R_z, where R_a is defined as the arithmetical mean deviation of the assessed surface pattern (arithmetic average roughness) [62] and Rz is the average among maximum peak to valley height within S, determined within a single sampling length (Rz_i) [62], as detailed in the equations shown in the Supplementary materials.

The presence of binder and dye residues was checked by monitoring the typical vibrations of each paint exploiting external reflection FTIR spectroscopy (ER-FTIR), using a portable FTIR spectrophotometer Alpha Bruker equipped with a front reflection module and OPUS software. For spray paints, the C=O stretching vibration of esters at 1727 cm^{-1} was monitored, while the bands of dyes visible in the fingerprint region were considered for felt-tip pens. An integrated videocamera allowed to define exactly the sample area to be analysed. The instrument operates in the frequency range of near and mid-infrared 7000–400 cm^{-1} with a measurement spot of 6 mm in diameter. 128 scans were acquired at a resolution of 4 cm^{-1}. Kramers–Kronig algorithm was applied to the spectra to correct spectral distortions.

The surface temperature on the treated area was monitored with IR thermocamera Optris PI400 (spectral range 9–13 μm, thermal sensitivity of 0.08 K, temperature range from − 20 to 900 °C, frame rate 80 Hz and resolution of 382×288 pixels). The measurement setup allowed to achieve a close up shot at approx. 20 cm from the treatment plane, with an angle of 45°, so the average pixel size is about 0.3 mm (the laser spot size is 110 μm). The emissivity of the surface was maintained constant at the average emissivity of the marble at 0.9 [63–65] during the whole acquisition. The response time of the IR

thermocamera is 11 ms, so the detected temperature is an average in time of that induced by the pulsed radiation (100 ns) [66]. The repetition frequency of laser pulses ranges from 40 to 200 kHz, influencing the monitored surface temperature. The surface temperature was monitored during all the treatment phases (before, during and after the laser radiation). The recording of the surface temperature before irradiation is essential to evaluate the time to return to the initial base temperature after the laser source has been turned off, and to check the heat diffusion in the surrounding area of the treatment.

In order to check possible modification of the marble structure after laser ablation, morphological analyses were performed on samples in cross section, by means of a SEM–EDS electronic microscope (ZEISS EVO MA 15) with W filament equipped with analytical system in dispersion of energy EDS/SDD, Oxford Ultimax 40 (40 mm^2 with resolution 127 eV @5.9 keV) with Aztec 5.0 SP1 software. The measurements were performed with the following operative conditions: an acceleration potential of 15 kV, 500 pA beam current, working distance comprised between 9–8.5 mm; 20 s live time as acquisition rate useful to archive at least 600.000 cts, on Co standard, process time 4 for point analyses.

Results

Observation of the surface

Visible images of the surfaces irradiated by different operative modes are shown in Tables 2 and 3. In Fig. 5, a comparison of stereomicroscopic images is presented in relation with the operative modes. With the same P_N, the cleaning tests on FB show a progressive thinning of the black paint with the increase of the repetition frequency, but none of them led to the complete removal of the paint layer. The corresponding laser parameters resulted in partial ablation of the paint on FR, while no effective thinning of the varnish was observed on MR, which instead appeared affected by a slight blackening due to the formation of small black spots. On MB, a gradual increase in the removal of the paint layer was observed with increasing P_N and repetition frequency. The stereomicroscope observation clearly showed paint remnants on the surface irradiated with the *M* mode, while shadows were visible underneath all the surfaces, which were inaccessible to laser. However, it is worthwhile to notice that the apparently more efficient paint removal is achieved with the operative mode *N*, exploiting intermediate laser parameters.

Colour changes

The global colour changes (ΔE), after painting (t1) and after cleaning (t2), are reported in the boxplots of Fig. 6 for the following operative modes: *E, F, G, H,* and *I* for

Suzuki *et al. Heritage Science*   (2023) 11:132

Page 11 of 20
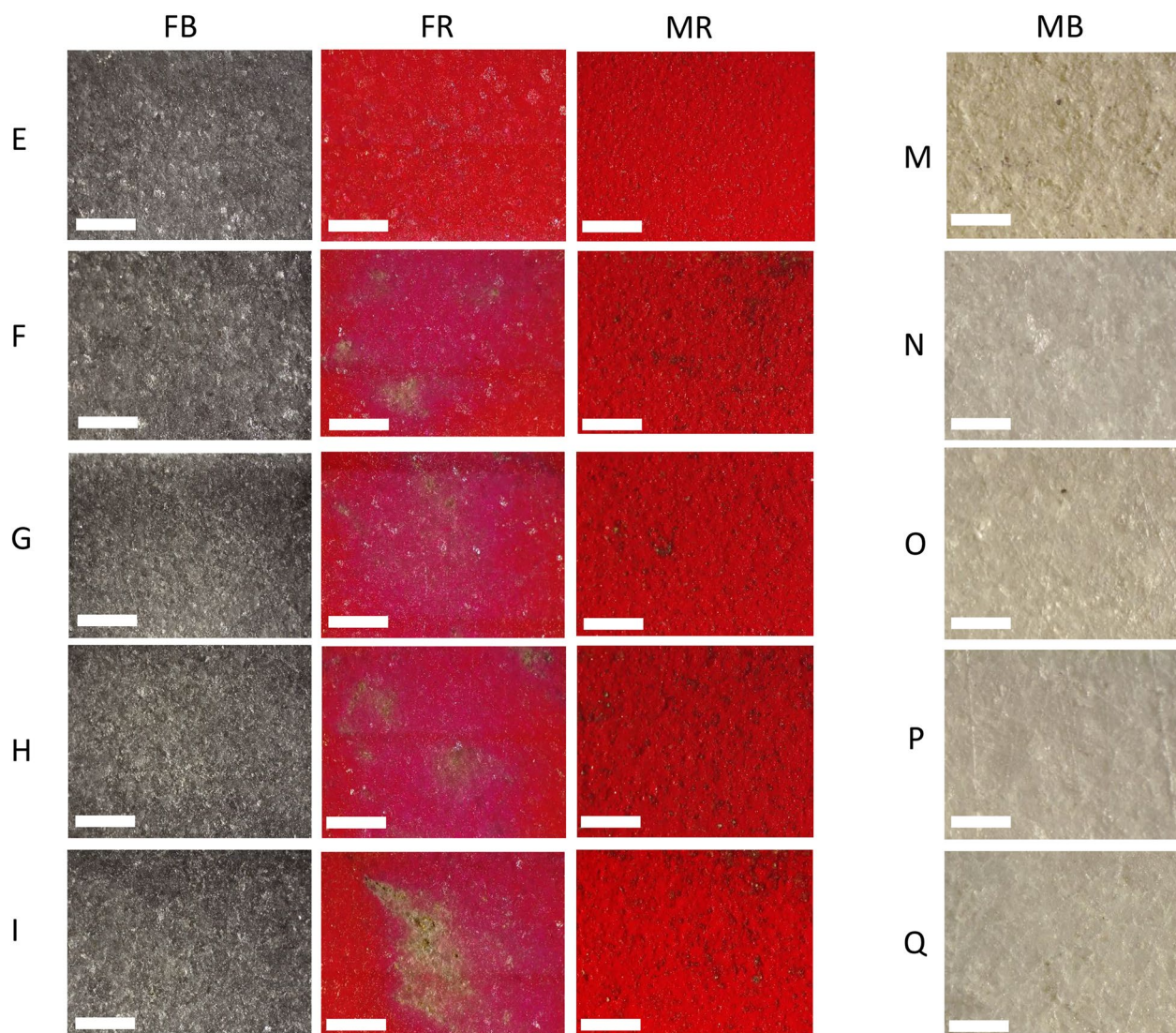
Fig. 5 Stereomicroscope images of the surfaces after cleaning with the *E-I* (for FB, FR and MR) and *M-Q* (MB) operative modes. The bar corresponds to 2 mm

FB, FR and MR; *M, N, O, P* and *Q* for MB. Overall, ΔE slightly diminished with the increase of the repetition frequency, except for MR where no significant cleaning was achieved, partially confirming the visible results by macro and stereomicroscope investigations. However, in FR the trend of ΔE values is not linear with the repetition frequency (see ΔE of *H* test in Fig. 6). Regarding colour coordinates (reported in Additional file 1: Fig. S3) in FB, FR and MB the colour change is mainly affected by $\Delta L^* < 0$ producing darkening, followed by slight reddish hue ($\Delta a^* \geq 0$) observed on FR, and a slight yellowing ($\Delta b^* > 0$) observed on FB and MB. The strongest ΔE decrease with the increase of repetition frequency was detected in MB.

Surface pattern control

The results of the surface morphology evaluation are reported for few significant cases and operative modes; however, all the treatments have been checked. Figure 7 shows the 3D map reconstruction for the surfaces painted with FB and MB and irradiated following the operative modes *I* and *N* respectively, which correspond to the best cleaning based on visual observation, colorimetric measurements (see sub-sections "Observation of the surface" and "Colour changes", respectively) and FTIR results (vide infra). In both cases, the left side of the image corresponds to the treated area (t2) whilst the right side is the painted, untreated area (t1). In Fig. 7b and d, the effect of the laser treatment

Suzuki *et al. Heritage Science*   (2023) 11:132

Page 12 of 20
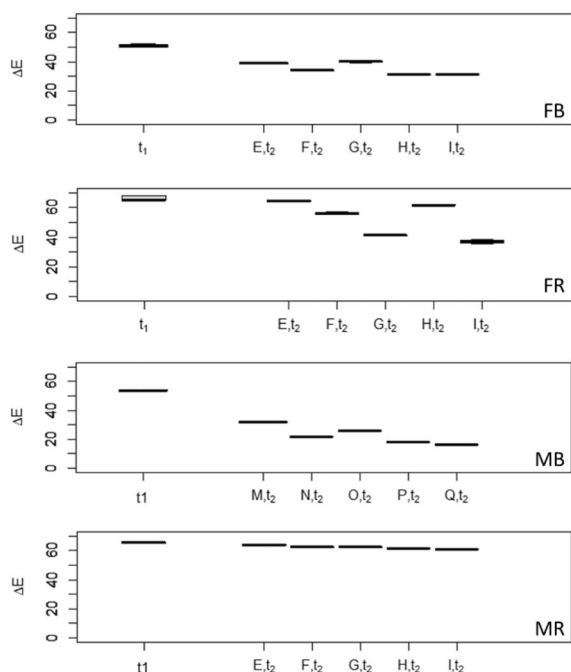
Fig. 6 Boxplot of the colour variation ΔE for FB, FR, MB and MR after the graffiti paint (t1) and after the cleaning (t2), with respect to each unpainted area (t0)

on the surface pattern is represented by the elevation map taking as zero reference the maximum of the untreated (painted) area t1. The amount of the material removed is evaluated on the z-axis. The z = 0 is referred to the maximum elevation on the area before the laser treatment, so the negative values of z indicate the level of material that has been removed. For effects evaluation, the roughness values for all the tests are reported for the pristine surface (t0), painted surface (t1) and treated surface (t2) and showed in Table 4.

The painted surfaces (t1) show *Ra* and *Rz* values lower than the corresponding pristine surface (t0) and laser treated surfaces (t2). Effective removal is observed when roughness of t2 approaches values of t0; this is very clear for the marker FB while for FR an increase in *Rz* is detected, suggesting localized marble abrasion likely due to the presence of dark veins in the marble (Additional file 1: Fig. S4), which enhance the absorption of laser radiation. For the spray paints, the *Ra* and *Rz* values for MB show some differences among treated (t2) and untreated areas (t1) for modes *M, N* and *Q*, where *M* and *Q* correspond to the operating modes with the mildest and most extreme parameters, respectively. The smallest difference between t2 and t0 is observed for *N* operative mode, suggesting an effective thinning of the paint. Instead, roughness values for MR were not reported since no effective ablation was observed on such paint.

ER-FTIR spectroscopy

On areas painted with permanent felt-tip pens, compared to the unpainted marble, the paint is detected as weak bands in the fingerprint region (Fig. 8 and Additional file 1: Fig. S5), as a result of the thin superficial layer of colour (Fig. 1). All the cleaning operating modes are associated with the complete disappearance of absorption bands between 1400 and 1000 cm^{-1}, related to both binder and dye as reported in Sect. "Characterization of paints", which suggests removal of the paint from the surface, with exception of *E* (40 W, 40 kHz). Indeed, as shown in Fig. 8, very weak bands are still detected on areas treated with the mildest operating mode.

Reflection FT-IR analyses on MB suggest that none of the operating modes was able to completely remove the paint from the surfaces, as deducible from the comparison of the C=O stretching bands at 1726 cm^{-1}, characteristic of esters and attributed to the alkyd-resin (Fig. 9). However, it is interesting to note that on MB the *N* mode showed the strongest depletion of peak intensities attributed to the alkyd resin, which is in accordance with the marked thinning of the paint visually observable (Fig. 5). On MR no depletion of alkyd-resin is observed (data not reported), in fact no cleaning effects were observed in any laser tests.

Temperature monitoring

The parameter t_R, indicated in Fig. 10, is related to the slope of the curve (temperature rising rate, R_t) that fits the registered data temperature since the initial instant (t_i = 0), when the laser is turned ON. The data are fitted by a concentrated constant model of the heating transmission, where t_R is one of the degrees of freedom together with T_∞.

The highest temperature registered during monitoring (T_{max}) for each operative mode is reported in Table 5 together with the R_t. For all the operative modes, the T_{max} rises as the P_N and the repetition frequency (f_R) increases. In FB, FR and MR, the lowest values of T_{max} are recorded with *E* (lowest P_N and repetition frequency), while the highest ones ($\geq$ 300 °C) occur as power increases (mode *G-I*), especially on FB. For MB, similar values of T_{max} are observed in *M* and *N*, while slightly increasing T_{max} and similar t_R are recorded from *O* to *Q*. The R_t depends on the interaction of the laser radiation with the material. For FB the R_t seems to show a dependence on threshold effect of f_R: under 80 kHz, R_t is independent from P, while over 80 kHz it increases with the power.

For MB, instead, the R_t decreases as f_R increases at constant power (5 kW), while the behaviour of R_t is not clear at constant frequency (80 kHz). In the case of red pigments, FR and MR, the R_t depends on both P and f_R, with no clear trend.
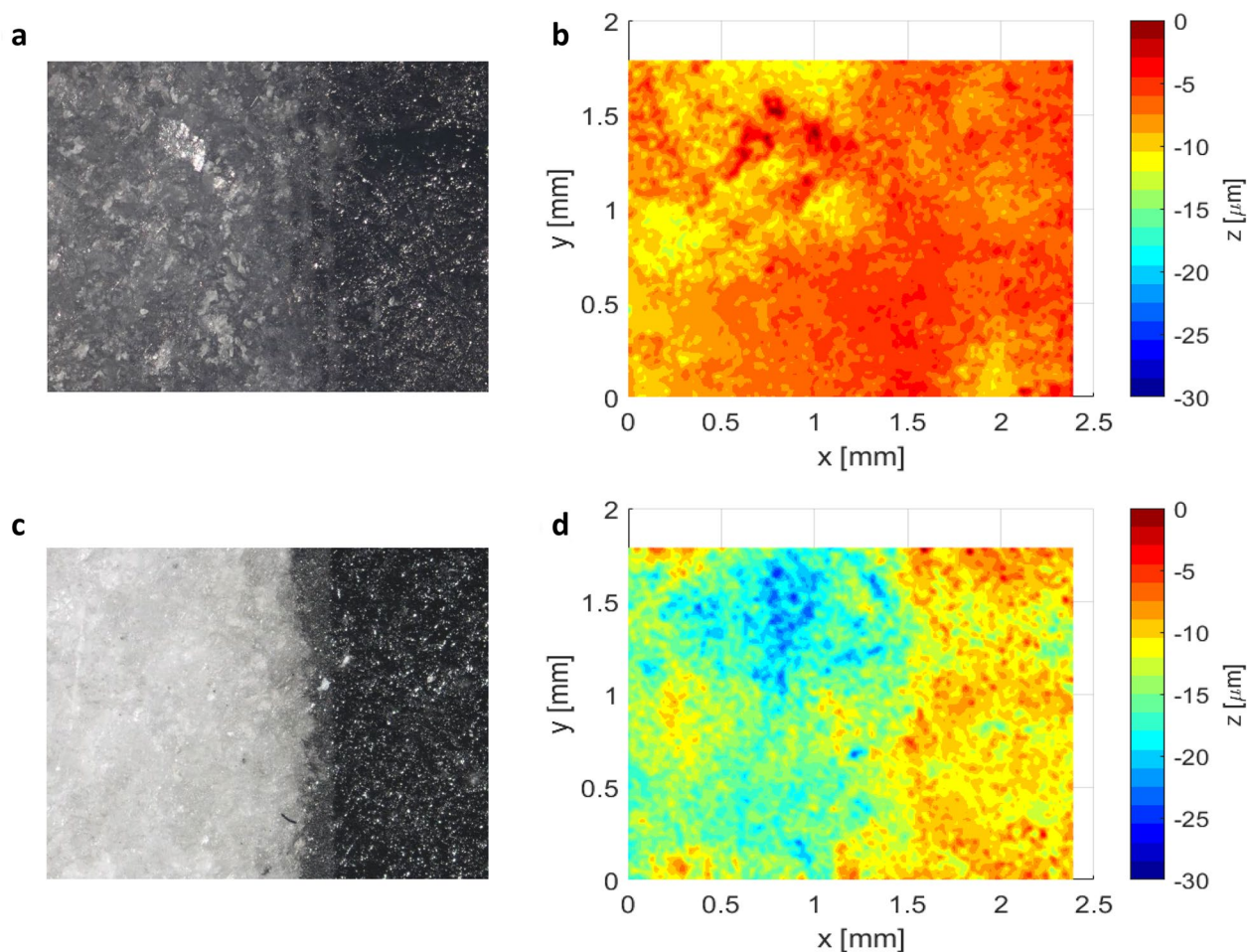
Fig. 7 Up: FB cleaned with the operative mode *I* under optical microscope (**a**) and its 3D elevation map (**b**). Bottom: MB cleaned with the operative mode *N* under optical microscope (**c**) and its 3D elevation map (**d**)

SEM–EDS

Possible modifications of the marble after laser ablation were evaluated by observing with SEM–EDS in cross section the area associated to the lowest surface temperature (MB, mode *N*) and the area that reached the highest surface temperature (MR, mode *F*). The marble underneath the paint in untreated areas does not seem to show morphological differences compared to the laser-treated marble, neither after reaching the lowest surface temperature (Fig. 11a-b, T = 106.7 °C) nor the highest (Fig. 11c-d, T = 359.2 °C).
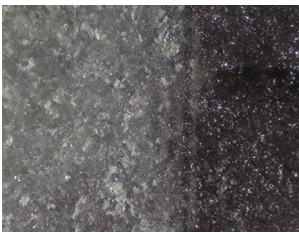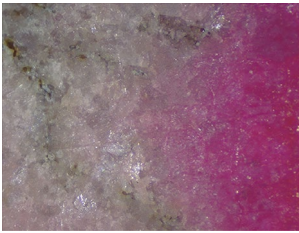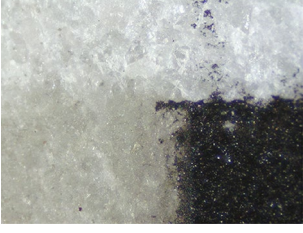
Discussion

The surface characterization via optical microscopy, colour measurements and spectroscopic investigations revealed different cleaning efficiency depending on the characteristics of the paint and on the laser settings. The effects of the laser treatment were also characterized by thermal monitoring and surface pattern evaluation. As a general remark, none of the cleaning tests resulted in a full recovery of the colorimetric parameters of the pristine marble (Fig. 6 and Additional file 1: Fig. S3), while roughness evaluation revealed a successful return of *Ra* and *Rz* to pristine surface values (Table 4). The spectroscopic investigation of the surfaces revealed some residues of the alkyd binder on MB (Fig. 9) and no residues of markers (FB and FR) (Fig. 8). Nevertheless, the cross sections of all the mock-ups before laser cleaning reveal a certain degree of paint penetration into the marble (Fig. 1). Since no cleaning method is without side effects, all of this information must be balanced as a trade-off to achieve effective removal with minimal side effect (abrasion). Indeed, in the case of laser treatment, due to the superficial nature of the method, it is impossible to totally remove the graffiti paint due to its penetration in the bulk without causing abrasion of the marble itself.

For black colours, better efficiency was generally observed compared to reds, as shown by the images

Suzuki *et al. Heritage Science*   (2023) 11:132

Page 14 of 20

Table 4 R_a and R_z parameters on FB, FR and MB treated using the operative mode *I*, *G* and *N*, respectively. t0: unpainted; t1: painted; t2: treated

Paint	Mode	t0		t1		t2		Microscope photo (4x)
		Ra [μm]	Rz [μm]	Ra [μm]	Rz [μm]	Ra [μm]	Rz [μm]	
FB	*I*	1.2	13.9	0.95	10.2	1.2	13.8	
FR	*G*	2.9	19.2	0.77	19.2	0.73	22.7	
MB	*M*	3.5	22.2	1.8	14.4	1.5	16.6	
MB	*Q*	1.7	12.3	2.6	11.0	1.3	11.4	
MB	*N*	2.7	24.3	4.4	23.8	5.5	24.8	

under the microscope (Fig. 5). The best thinning visually observed on FB was achieved with the maximum power and the maximum frequency (*I* operative mode, Table 2), which induced a surface heating up to about 350 °C (Table 5), while on MB the apparently more efficient cleaning was obtained with intermediate settings (*N*) inducing lower heating (about 107 °C, Table 5). On FB, with *I* setting, no paint residues were detected by FTIR analysis of the surfaces (Additional file 1: Fig. S5). However, the absence of bands related to the paint in the operating modes *F–H* is in disagreement with the colour still visible on these areas (Fig. 5), and confirmed by colorimetric results (Fig. 6 and Additional file 1: Fig. S3a), suggesting that the paint depletion was superficial.

Suzuki *et al. Heritage Science*   (2023) 11:132

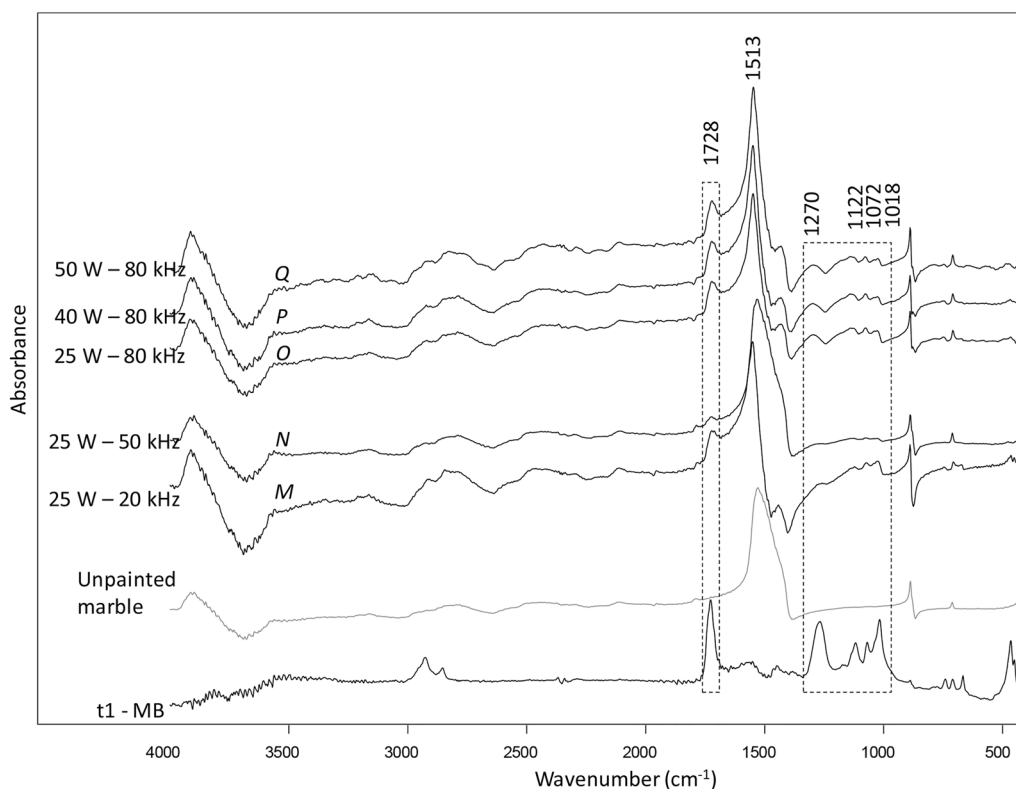Page 15 of 20
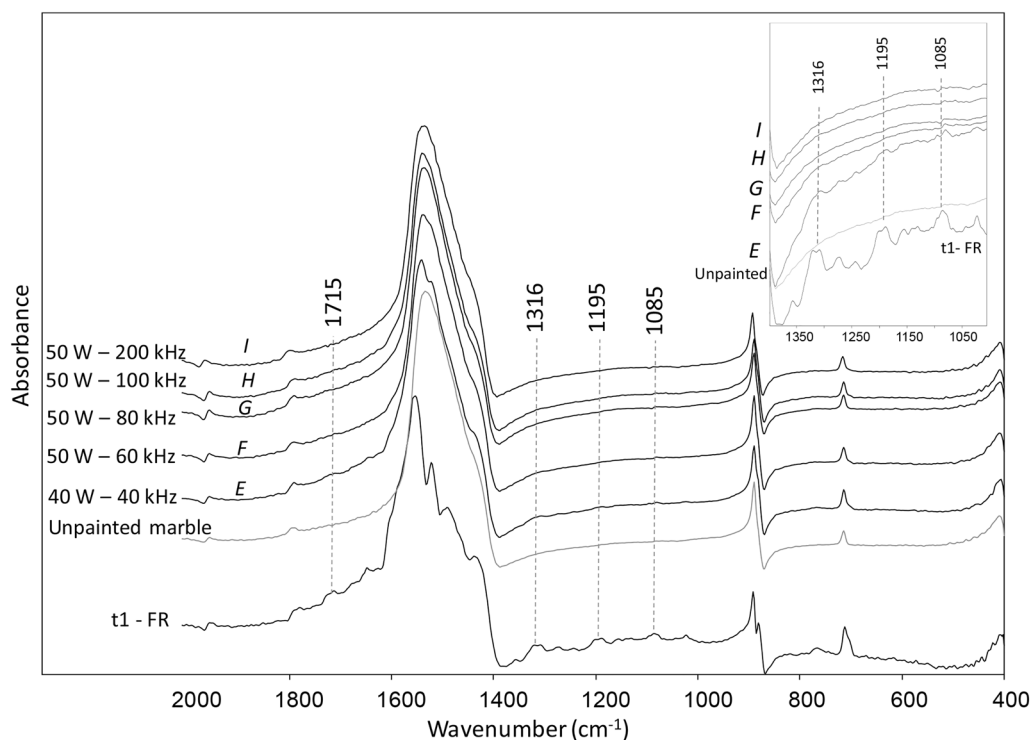
Fig. 8 FTIR spectra after elaboration with K-K algorithm of FR-painted surfaces cleaned with *E-I* operative modes. Reference spectra of the FR paint on marble (t1-FR) and of the unpainted marble are also reported. The dashed lines highlight the monitored vibrational bands, indicative of paint remains. The inset highlights the depletion of marker vibrational bands with the different cleaning modes

Indeed, due to penetration underneath the surface, the paint may be detected by the naked eye but not probed by reflection FTIR. In addition, FB roughness increased after laser treatment compared to the painted, untreated surface (t1), returning to the initial value of the unpainted surface (t0, Fig. 7b and Table 4). This may suggest that the cleaning was efficient on the surface, as also confirmed by FTIR spectra (Additional file 1: Fig. S5) and that no mechanical damage at the marble surface was produced. On MB, no evident alteration of the substrate at high magnification was observed for all the treatments, as shown by optical and electron microscopy, and no significant variations of roughness were observed on the surface treated with mode *N* (Table 4). However, some residues of paint remained after irradiation, shown as a slight yellowing from colorimetric coordinates (increase of the value of b*, Additional file 1: Fig. S3c); this yellowing is of different nature from what has been observed in the laser-induced discoloration of encrusted marble [12, 17, 67]. Indeed, FTIR spectra still detect the presence of alkyd resin residues after all laser treatments on MB (Fig. 9), but *N* mode shows the strongest depletion of peak intensities attributed to the alkyd resin.

Regarding FR, visual observations and roughness measurements show that it was almost impossible to

effectively remove the paint (Fig. 6) without damage. In fact, the presence of veins in the marble, covered by paint, caused damage to the substrate in terms of abrasion (Table 4). All the operative modes with repetition rate above 60 kHz induced a consistent heat accumulation as revealed by the reaching of temperatures above 200 °C (Table 5). These tests caused inhomogeneous thinning of the paint and a colour shift towards red (Fig. 5 and Additional file 1: Fig. S3b) which can be correlated to the presence of the two yellow and pink dyes revealed by TLC (Fig. 2) and characterized by vibrational spectroscopies. The colour shift can be associated to the selective thermal decomposition of the yellow azo-dye, which may occur at temperature above 200 °C [68], reached in operative modes *F-I*, leaving unaltered the pink Rhodamine 6G which decomposes at 492 °C [69].

Similarly, on MR all the operative modes reported were ineffective and black spots were progressively observed more numerous with increasing power and repetition frequency (Fig. 5), hence increase of surface temperature, in particular for modes *F-I*. This observation suggests that MR cannot be removed unless laser settings inducing combustion of the paint are used. A confirmation about this extreme thermal effect with a consequent removal of the paint is described by a dedicated experiment

Suzuki *et al. Heritage Science*   (2023) 11:132

Page 16 of 20

Fig. 9 FTIR spectra after elaboration with K-K algorithm of MB-painted surfaces cleaned with *M-Q* operative modes. Reference spectra of the MB paint on marble (t1), and of the unpainted marble are also reported. The dashed squares highlight the monitored vibrational bands, indicative of paint remains
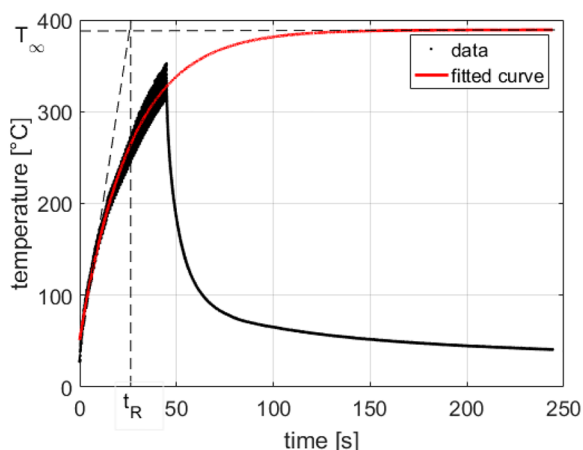
Fig. 10 Typical trend of heating/cooling behaviour (point) with data fitting (red line). The plot is referred to FB graffiti paintings with operative mode *G*. T_∞ is the asymptotic behaviour of the heat induced by laser radiation on the surface, and it indicates the maximum temperature value that is reached at infinity; t_R is the increase of surface temperature over ambient temperature, induced by laser radiation

(Additional file 1: Fig. S6), but at the same time a severe damage on the substrate was observed (bleaching).

Two prominent laser/material interactions can be deduced in consideration of laser settings and paints. The main laser parameters are the spot overlap, strictly bound to the combination of repetition rate (frequency) and scan speed, and the peak power (energy dose). The main material characteristic is the absorption at the specific laser wavelength, whose values determine the ablation threshold. The high reflectivity of both red paints at the laser wavelength used [46] prevents ablation of the paint layer, being the main responsible for the ineffective removal of these red colours. In turn, on MB the high absorption of the radiation by the carbon black pigment favoured the ablation of the paint (Fig. 5) with relatively low surface heating (T_{max} 100–174 °C) and short irradiation time required (3–5 s instead of 40 s for the thinning of FB). Instead, at high frequency the spot overlap becomes significant (Fig. 4), leading to a quasi-continuum nature of the laser radiation that produces severe surface heat accumulation with a consequent increase of the thermal effect. On the markers (FR e FB) this thermal effect can gradually degrade the paint as a result of partial decomposition of the dyes (Fig. 5). However, also in

Table 5 Surface temperatures data for each operative mode and for each mock-up

Operative mode (P [kW]; f_R [kHz])	FB (black)		FR (red)		MB (black)		MR (red)	
	T_{max} [°C]	R_t [°C/s]	T_{max} [°C]	R_t [°C/s]	T_{max} [°C]	R_t [°C/s]	T_{max} [°C]	R_t [°C/s]
E (10; 40)	199.6	7.4	178	6.29	–		207.5	13.65
F (8; 60)	243.8	7.4	290.7	10.55	–		359.2	9.41
G (6.3; 80)	347.4	12.64	281.1	14.62	–		266.2	15.95
H (5; 100)	352.3	11.70	228.8	11.61	–		339.9	8.08
I (7; 200)	344	13.29	344	18.32	–		300.6	7.98
M (5; 20)	–		–		105.9	15.85	–	
N (5; 50)	–		–		106.7	10.29	–	
O (3.1, 80)	–		–		152.9	10.30	–	
P (5, 80)	–		–		156.5	9.98	–	
Q (6.3, 80)	–		–		174.2	12.09	–	

Scan size and spot size are the same for each operative mode, 110 μm and 15 mm, respectively. P: peak power; f_R: repetition frequency; T_{max}: highest temperature reached for each operative mode; R_t: temperature rising rate
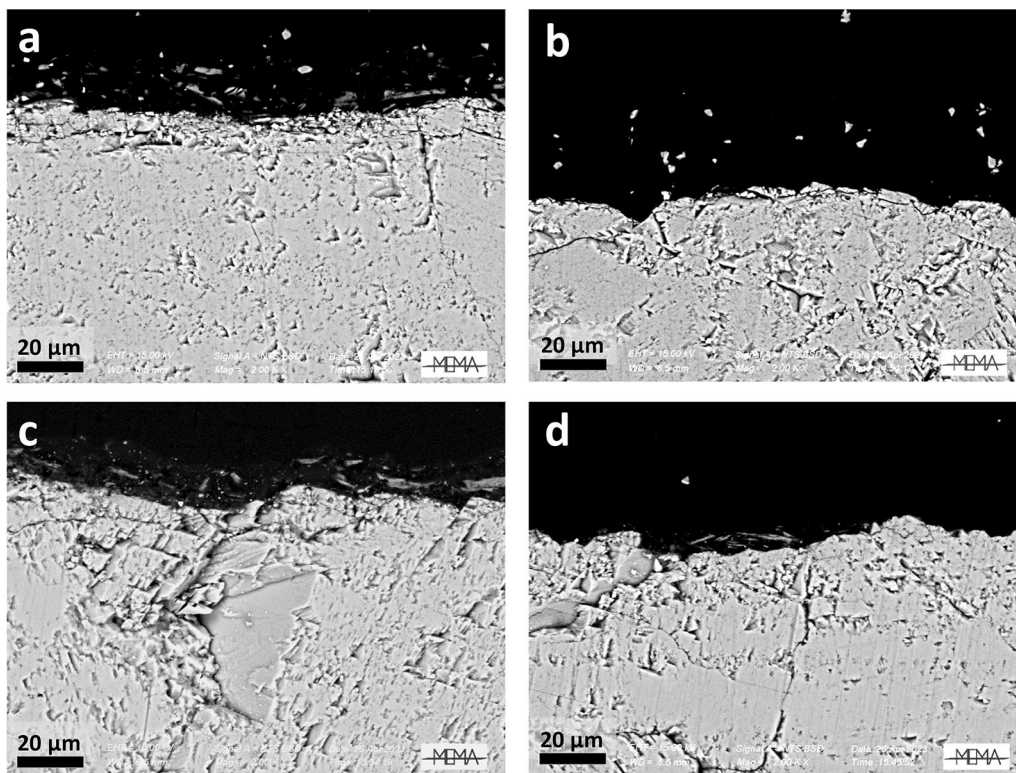
Fig. 11 SEM–EDS images of cross sections of representative zones in sample MB, mode *N* before (**a**) and after laser treatment (**b**) and in sample MR, mode F before (**c**) and after laser treatment (**d**). The white spots on the surface in image (**b**) are silicon carbide due to polishing (checked with EDS probe, spectrum not shown)

this operative modality, localized abrasion processes can occur due to the presence of veins in the marble under the thinned paint (see FR row on Table 4). Overall, predominant ablative effects were generally observed below 150 °C on MB with relatively low frequencies, while predominant thermal effects occurred above this temperature and were observed on MR, FR and FB with higher repetition frequencies.

Suzuki *et al. Heritage Science*   (2023) 11:132

Page 18 of 20

Conclusions

With the common flash pumped solid state pulsed laser, the established evaluation method is based on the selection of the energy per pulse and the beam diameter, which determines the fluence that is proportional to the intensity of the laser effect in a certain range of linearity. Initially, very low pulse energy and a large beam size should be applied and gradually adjusted to achieve the fluence that permits an efficient cleaning without damaging. This approach may not be applicable when using a fiber laser system, because of the scanning system and therefore additional parameters that influence the efficiency of paint removal. In this paper, a first insight into the ablation and thermal effects of Yb:YAG fiber laser system was provided on a selection of paints from felt-tip pens and sprays, identifying the frequency and average power supplied as the key parameters that influence the behaviour of this laser. Moreover, the interaction of the laser radiation with the materials tested was investigated. Without the necessity to change the pulse duration and thanks to the operation at high frequency with a scanning system, this laser can create either a predominantly photomechanical or thermal effect, depending on the laser setting and the absorption values of the specific laser radiation by the materials. These two aspects might be very useful for the removal of graffiti, but it is necessary to consider the damage threshold of the specific substrate, which is different based on the mineralogy and chemistry of the stone. Apart from the clear damage caused by excessive ablation (abrasion of the substrate), heat accumulation and prominent thermal effects could also cause decomposition and partial melting of the stone, as well as mechanical stress due to thermal expansion/contraction of crystals. For this reason, this research will be followed by a specific study on the possible detrimental effects on different polymineralic substrates varying the laser settings, such as the size of the scan and the beam diameter. Best results were obtained for the gradual thinning of the black permanent marker and for the efficient cleaning of the black spray paint. Even in the best cleaning results, paint residues were detected, confirming that the use of the laser as a standalone approach is not efficient for the total removal of the graffiti paints; instead, it should be considered as a crucial preliminary step that can be integrated with a second step of chemical cleaning as the amount of paint is reduced and the risk of migration of the colour is mitigated.

The ideal starting point for a new cleaning test would be a condition of low power and combination of frequency and scan speed that permits to have contiguous spots. This condition would help at first to assess the type of interaction with the material to remove. In particular, if a certain ablation is observed, then the frequency can be reduced and the power increased for a more efficient ablative effect; this can be done if the damage threshold is not exceeded. Conversely, if the interaction with the laser beam is weak then both the frequency and power can be increased to see if a more thermal action can be effective for the desired cleaning. This strategy can only be applied if the specific substrate to be treated is not damaged due to heating.

Abbreviations

FB	Felt pen black
FR	Felt pen red
MB	Marker black
MR	Marker red
BF	Brush fill
BW	Brush width
P_N	Average power
P	Peak power
T_{max}	Highest temperature
f_R	Repetition frequency
R_t	Temperature rising rate
t_R	Surface temperature rise
T_∞	Asymptotic temperature value

Supplementary Information

The online version contains supplementary material available at https://doi.org/10.1186/s40494-023-00966-9.

Additional file 1: Fig. S1. Raman spectrum of the black spot not eluted from FB. The spectral profile suggests the presence of carbon black. **Fig. S2**. FTIR-ATR spectra ofFR and FB;MR and MB.. **Fig. S3**. Colour coordinatesfor FB in, FR inMB inand MR inof the marble, graffiti paintand their cleaning tests. **Fig. S4**. a) The pristine marble before the application of the FR marker and b) painted marble after some of the laser cleaning tests with the maximum power, varying the frequency. The inhomogeneous laser cleaning clearly follows the dark veins pattern of the marble. **Fig. S5**. Reflection FTIR spectra after elaboration with K-K algorithm of FB-painted surfaces cleaned with E-H operative modes. Reference spectra of the FB paint on marbleand of the unpainted marble are also reported. The dashed lines highlight the monitored vibrational bands, indicative of paint remains. The inset highlights the depletion of marker vibrational bands with the different cleaning modes. **Fig. S6.** Optical microscope imageof 4 contiguous laser treatment tests on MR with operative mode *G* with the only difference being the size dimension of 5 mm. Equations and details on colorimetric and roughness measurements.

Author contributions

AS contributed to the preparation of specimens and to the laser tests, to the acquisition and interpretation of FTIR, Raman, TLC, XRF, optical microscope and thermal data, and she has drafted the paper and contributed to the discussion of the results and the manuscript revision. CR contributed to laser tests, surface pattern control and thermal analysis. He contributed to the conceptualization, writing and revision of this paper. MR contributed to the acquisition and interpretation of the Raman spectra, she has revised the paper and approved the submitted version. SV contributed to the preparation of specimens and to the conceptualization of the paper. She has revised the manuscript and approved the submitted version. BS performed ATR-FTIR analyses of the paints, interpreted all the FTIR spectra obtained in this study and contributed to the decisions and discussion of the results. She contributed to the conceptualization of the paper and was a major contributor to the

writing and reviewing of the manuscript. All authors read and approved the final manuscript.

Availability of data and materials
The datasets used and analysed during the current study are available from the corresponding author on reasonable request.

Declarations

Competing interests
The authors declare that they have no competing interests.

Author details
[1]Institute of Heritage Science, National Research Council (CNR-ISPC), Via Madonna del Piano 10, 50019 Sesto Fiorentino (Florence), Italy. [2]Department of Chemistry "Ugo Schiff", University of Florence, Via della Lastruccia 13, 50019 Sesto Fiorentino (Florence), Italy.

References

1. Gomes V, Dionísio A, Pozo-Antonio JS. Conservation strategies against graffiti vandalism on Cultural Heritage stones: protective coatings and cleaning methods. Prog Org Coat. 2017;113:90–109. https://doi.org/10.1016/j.porgcoat.2017.08.010.
2. Pozo-Antonio JS, Rivas T, López AJ, Fiorucci MP, Ramil A. Effectiveness of granite cleaning procedures in cultural heritage: a review. Sci Total Environ. 2016;571:1017–28.
3. Sanmartín P, Cappitelli F, Mitchell R. Current methods of graffiti removal: a review. Constr Build Mater. 2014;71:363–74. https://doi.org/10.1016/j.conbuildmat.2014.08.093.
4. Macchia A, Capriotti S, Rivaroli L, Ruffolo SA, La Russa MF. Protection of urban art painting: a laboratory study. Polym. 2022;14(1):162–8. https://doi.org/10.3390/polym14010162.
5. Macchia A, Castro M, Curbelo C, Rivaroli L, Capriotti S, Vieira E, Moreira P, Ruffolo SA, La Russa MF. Methods and products for the conservation of vandalized urban art murals. Coatings. 2021;11:1304. https://doi.org/10.3390/coatings11111304.
6. Macchia A, Ruffolo SA, Rivaroli L, Malagodi M, Licchelli M, Rovella N, Randazzo L, La Russa ML. Comparative study of protective coatings for the conservation of Urban Art. J Cult Herit. 2020;41:232–7.
7. Weaver ME. Removing Graffiti from Historic Masonry. Preservation Brief No. 38, National Park Service, Technical Preservation Services, Washington DC, 1995. https://www.nps.gov/orgs/1739/upload/preservation-brief-38-graffiti.pdf. Accessed 8 Feb 2023.
8. Careddu N, Akkoyun O. An investigation on the efficacy of water-jet technology for graffiti cleaning. J Cult Herit. 2016;19:426–34. https://doi.org/10.1016/j.culher.2015.11.009.
9. Pozo-Antonio JS, Rivas T, Fiorucci MP, Lopez AJ, Ramil A. Effectiveness and harmfulness evaluation of graffiti cleaning by mechanical, chemical and laser procedures on granite. Microchem J. 2016;125:1–9.
10. Pozo-Antonio JS, López L, Dionísio A, Rivas T. A study on the suitability of mechanical soft-abrasive blasting methods to extract graffiti paints on ornamental stones. Coatings. 2018;8:335–54.
11. Carvalhão M, Dionisio A. Evaluation of mechanical soft-abrasive blasting and chemical cleaning methods on alkyd-paint graffiti made on calcareous stones. J Cult Herit. 2015;16:579–90.
12. Ortiz P, Antúnez V, Ortiz R, Martín JM, Gómez MA, Hortal AR, Martínez-Haya B. Comparative study of pulsed laser cleaning applied to weathered marble surfaces. Appl Surf Sci. 2013;283:193–201. https://doi.org/10.1016/j.apsusc.2013.06.081.
13. Urquhart D. The treatment of graffiti on historic surfaces. Advice on graffiti removal procedures, anti-graffiti coatings and alternative strategies, in: Historic Scotland Technical Advice Note No. 18, Historic Scotland, Edinburgh, 1999.
14. Musolino M, Aricò F, Tundo P. An innovative and sustainable approach to spray paint graffiti removal from Istrian stone through the silica sol-gel chemistry: a preliminary assessment. J Cult Herit. 2019;36:268–74. https://doi.org/10.1016/j.culher.2018.08.003.
15. Giorgi R, Baglioni M, Baglioni P. Nanofluids and chemical highly retentive hydrogels for controlled and selective removal of over paintings and undesired graffiti from street art. Anal Bioanal Chem. 2017;409:3707–12. https://doi.org/10.1007/s00216-017-0357-z.
16. Baglioni M, Poggi G, Jaidar Benavides Y, Martínez Camacho F, Giorgi R, Baglioni P. Nanostructured fluids for the removal of graffiti—a survey on 17 commercial spray-can paints. J Cult Herit. 2018;34:218–26. https://doi.org/10.1016/j.culher.2018.04.016.
17. Pouli P, Oujja M, Castillejo M. Practical issues in laser cleaning of stone and painted artefacts: optimisation procedures and side effects. Appl Phys A. 2012;106:447–64. https://doi.org/10.1007/s00339-011-6696-2.
18. Costela A, García-Moreno I, Gómez C, Caballero O, Sastre R. Cleaning grafftis on urban buildings by use of second and third harmonic wavelength of a Nd:YAG laser: a comparative study. Appl Surf Sci. 2003;207:86–99.
19. Gómez C, Costela A, García-Moreno I, Sastre R. Comparative study between IR and UV laser radiation applied to the removal of graffitis on urban buildings. Appl Surf Sci. 2006;252:2782–93. https://doi.org/10.1016/j.apsusc.2005.04.051.
20. Ramil A, Pozo-Antonio JS, Fiorucci MP, López AJ, Rivas T. Detection of the optimal laser fluence ranges to clean graffiti on silicates. Constr Build Mater. 2017;148:122–30. https://doi.org/10.1016/j.conbuildmat.2017.05.035.
21. Pozo-Antonio JS, Papanikolaou A, Melessanaki K, Rivas T, Pouli P. Laser-assisted removal of graffiti from granite: advantages of the simultaneous use of two wavelengths. Coatings. 2018;8:124–44. https://doi.org/10.3390/coatings8040124.
22. Andriani SE, Catalano IM, Daurelio G, Albanese A. Marker and pen graffiti cleaning on diverse calcareous stones by different laser techniques. Presented at the XVI International Symposium on Gas Flow, Chemical Lasers, and High-Power Lasers, Gmunden, Austria, 2006, p. 634636. https://doi.org/10.1117/12.739334.
23. Giusti C, Colombini MP, Lluveras-Tenorio A, La Nasa J, Striova J, Salvadori B. Graphic vandalism: multi-analytical evaluation of laser and chemical methods for the removal of spray paints. J Cult Herit. 2020;44:260–74. https://doi.org/10.1016/j.culher.2020.01.007.
24. Ricci C, Gambino F, Nervo M, Piccirillo A, Scarcella A, Zenucchini F, Pozo-Antonio JS. Developing new cleaning strategies of cultural heritage stones: are synergistic combinations of a low-toxic solvent ternary mixtures followed by laser the solution? Coatings. 2020;10:466–88. https://doi.org/10.3390/coatings10050466.
25. Ricci C, Gambino F, Nervo M, Piccirillo A, Scarcella A, Zenucchini F, Ramil A, Pozo-Antonio JS. Enhancement of graffiti removal from heritage stone by combining laser ablation and application of a solvent mixture. Constr Build Mater. 2020;262:119934–48. https://doi.org/10.1016/j.conbuildmat.2020.119934.
26. Salimbeni R, Pini R, Siano S. A variable pulse width Nd:YAG laser for conservation. J Cult Herit. 2003;4(1):72–6.
27. Siano S, Giamello M, Bartoli L, Mencaglia A, Parfenov V, Salimbeni R. Laser cleaning of stone by different laser pulse duration and wavelength. Laser Phys. 2008;18:27–36.
28. Fotakis C, Anglos D, Zafiropoulos V, Georgiou S, Tornari V. Lasers in the preservation of cultural heritage: principles and applications. London: Taylor & Francis Group; 2006. p. 336.
29. Brygo F, Dutouquet CH, Le Guern F, Oltra R, Semerok A, Weulersse JM. Laser fluence, repetition rate and pulse duration effects on paint ablation. Appl Surf Sci. 2006;252:2131–8. https://doi.org/10.1016/j.apsusc.2005.02.143.
30. Fiorucci MP, López AJ, Ramil A, Pozo S, Rivas T. Optimization of graffiti removal on natural stone by means of high repetition rate UV laser. Appl Surf Sci. 2013;278:268–72. https://doi.org/10.1016/j.apsusc.2012.10.092.
31. Rode AV, Baldwin KGH, Wain A, Madsen NR, Freeman D, Delaporte PH, Luther-Davies B. Ultrafast laser ablation for restoration of heritage

Suzuki *et al. Heritage Science*   (2023) 11:132

Page 20 of 20

objects. Appl Surf Sci. 2008;254:3137–46. https://doi.org/10.1016/j.apsusc.2007.10.106.

32. Nufern BS, Dong L. Fiber lasers. In: Handbook of solid-state lasers. Elsevier, 2013, pp. 403–462. https://doi.org/10.1533/9780857097507.2.403.

33. Addankia S, Amirib IS, Yupapin P. Review of optical fibers-introduction and applications in fiber lasers. Results Phys. 2018;10:743–50.

34. Dajnowski B, Dajnowski A. The use of new laser technology to precisely control the level of stone cleaning. In: Hughes J, Howind T, editors. Science and art: a future for stone: Proceedings of the 13th International Congress on the Deterioration and Conservation of Stone, Volume 2. Paisley: University of the West of Scotland; 2016. pp. 719–28.

35. Kaczkowski RA, Dajnowski BA, Vincenzi EP. From earth to outer space: laser cleaning semiprecious quartz and a novel application for meteoritic metal. In: Tagowski P, Walczak M, Pouli P editors. Lasers in the conservation of artworks XI: Proceedings of the International Conference LACONA XI, Krakow, Poland, 20–23 September 2016, 47–62. https://doi.org/10.12775/3875-4.03.

36. ANSA Latest news. https://www.ansa.it/english/news/2019/01/07/florence-beauty-angels-get-laser-to-remove-graffiti_7f282697-9dbc-43dc-b157-f58545bce097.html. Accessed 8 Feb 2023; You Tube. https://youtu.be/_okxLL7EKg0. Accessed 8 Feb 2023.

37. Suzuki A, Riminesi C, Salvadori B, Vettori S, Ricci M, Bartoli L, Zanini A. Graphic vandalism: preliminary cleaning tests on stone materials by (Yb:YAG) active fiber laser system. In: Siegesmund S and Middendorf B, editors. STONE 2020 monument and future: decay and conservation of stone—14th International Congress on the Deterioration and Conservation of Stone, Gottingen, Germany, 7–12 September 2020, 579–584.

38. Di Francia E, Lahoz R, Neff D, Rico V, Nuns N, Angelini E, Grassini S. Novel procedure for studying laser-surface material interactions during scanning laser ablation cleaning processes on Cu-based alloys. Appl Surf Sci. 2021;544:148820–8.

39. Fratini F, Rescic S. The stone materials of the historical architecture of Tuscany, Italy. Geol Soc Lond Special Publications. 2014;391:71–92. https://doi.org/10.1144/SP391.5.

40. Malesani P, Pecchioni E, Cantisani E, Fratini F. Geolithology and provenance of materials of some historical buildings and monuments on the center of Florence (Italy) Episodes. 2003; 26(3): 250–55.

41. RAL Colours. http://www.ral-farben.de. Accessed 8 Feb 2023

42. https://www.montanacolors.com/en/productos/mtn-94-aerosol-spray-paint. Accessed 8 Feb 2023.

43. Germinario G, van der Werf ID, Sabbatini L. Chemical characterisation of spray paints by a multi-analytical (Py/GC–MS, FTIR, μ-Raman) approach. Microchem J. 2016;124:929–39. https://doi.org/10.1016/j.microc.2015.04.016.

44. Germinario G, Garrappa S, D'Ambrosio V, van der Werf ID, Sabbatini L. Chemical composition of felt-tip pen inks. Anal Bioanal Chem. 2018;410:1079–94. https://doi.org/10.1007/s00216-017-0687-x.

45. Izzo FC, Vitale V, Fabbro C, Van Keulen H. Multi-analytical investigation on felt-tip pen inks: formulation and preliminary photo-degradation study. Microchem J. 2016;124:919–28. https://doi.org/10.1016/j.microc.2015.09.008.

46. Salvadori B, Del Colle M, Caciagli S, Cantisani E, Agostini B, Trafeli V, Fontana R, Striova J. Rimozione delle scritte a pennarello dalle superfici in marmo: approccio fisico-chimico. Atti del Convegno APLAR5: applicazioni laser nel restauro, Musei Vaticani, 18-20 settembre 2014. A cura di Anna Brunetto, Nardini Editore, 2017, pp. 121–130.

47. Pedna A, Giuntoli G, Rosi L, Frediani M, Sacchi B, Cantisani E, Colombini MP, Frediani P. Poly(lactic acid)-based polymers for the protection of monumental stone Heritage". Proceedings of the XXVIII Conference "Scienza e Beni Culturali, La conservazione del Patrimonio Architettonico all'aperto". Bressanone, Italy, 10–12 July 2012, pp. 489–498.

48. Cantisani E, Pecchioni E, Fratini F, Garzonio CA, Malesani P, Molli G. Thermal stress in the Apuan marbles: relationship between microstructure and petrophysical characteristics. Int J Rock Mech Min. 2009;46(1):128–37.

49. Montana Colors. https://www.montanacolors.com/downloads/tdsmtn94en.pdf. Accessed 8 Feb 2023.

50. Sodo A, Bicchieri M, Guiso M, Ricci MA, Ricci G. Raman investigations on marker pen inks. J Raman Spectrosc. 2012;43:1781–7.

51. Majoube M, Henry M. Fourier transform Raman and infrared and surface-enhanced Raman spectra for rhodamine 6G. Spectrochim Acta A Mol Biomol Spectrosc. 1991;47(9–10):1459–66.

52. Kumar CG, Poornima M, Anver B, Joveeta J, Sarma VUM, Ahmed K. Decolorization and biotransformation of triphenylmethane dye, methyl violet, by Aspergillus sp. Isolated from Ladakh, India. J Microbiol Biotechnol. 2011;21(3):267–73.

53. Watanabe H, Hayazawa N, Inouye Y, Kawata S. DFT vibrational calculations of Rhodamine 6G adsorbed on silver: analysis of tip-enhanced raman spectroscopy. J Phys Chem B. 2005;109:5012–20.

54. Herbst W, Hunger K. Industrial organic pigments. Production, properties and applications. WILEY-VCH Vergal GmbH & Co. KGaA, Weinheim, Germany, 2004, pp. 670.

55. Ploeger R, Scalarone D, Chiantore O. The characterization of commercial artists' alkyd paints. J Cul Herit. 2008;9:412–9. https://doi.org/10.1016/j.culher.2008.01.007.

56. Light for Art—Infinito Laser. http://www.lightforart.com/en/laser-infinito-en/. Accessed 8 Feb 2023.

57. Siano S, Salimbeni R. Advances in laser cleaning of artwork and objects of historical interest: the optimized pulse duration approach. Acc Chem Res. 2010;43:739–50. https://doi.org/10.1021/ar900190f.

58. Bargi M, Morigi MP, Fontana R, Pampaloni E, Striova J, Salvadori B. Efficiency evaluation of chemical and physical methods for the removal of spray paints from marble substrates. IOP Conf. Ser.: Mater. Sci. Eng. 2020; 949: 012027.

59. Dyer J, Verri G, Cupitt J. Multispectral Imaging in reflectance and photo-induced luminescence modes: a user manual, 2013. EU-Project Charisma http://www.britishmuseum.org/pdf/charisma-multispectral-imaging-manual-2013.pdf. Accessed 8 Feb 2023.

60. EN 15886:2010. Conservation of Cultural Property: Test Methods, Colour Measurement of Surfaces. European Committee for Standardization.

61. Barbetti I, Felici A, Magrini D, Manganelli Del Fà R, Riminesi C. Ultra close-range photogrammetry to assess the roughness of the wall painting surfaces after cleaning treatments. Int J Conserv Sci. 2013;4:525–34.

62. BS EN ISO 4287:2000, Geometrical product specification. Surface texture. Profile method. Terms, definitions and surface texture parameters.

63. ASTM C1371—04a 2010 Standard Test Method for Determination of Emittance of Materials, Near Room Temperature Using Portable Emissometers ASTM International West, Conshohocken PA.

64. Asdrubali F, Baldinelli G, Bianchi F, Presciutti A, Rossi F, Schiavoni S. Thermal and optical characterization of natural and artificial marble for roof and external floor installations. J Phys Conf Ser. 2015;655:012017–27.

65. Avdelidis NP, Moropoulou A. Emissivity considerations in building thermography. Energy Build. 2003;35(7):663–7. https://doi.org/10.1016/S0378-7788(02)00210-4.

66. Felici A, Riminesi C, Striova J, Bartoli L, Zanini A. Monitoraggio mediante imaging nell'infrarosso termico del riscaldamento indotto da laser durante la pulitura di superfici di intonaci dipinti. In: Brunetto A, Lanterna G, Mazzei B, editors. Atti del Convegno APLAR6: Applicazioni laser nel restauro, Firenze 14–16 settembre 2017. Nardini Editore, 2019, pp.161–72.

67. Samolik S, Walczak M, Plotek M, Sarzynski A, Pluska I, Marczak J. Investigation into the removal of graffiti on mineral supports: comparison of nano-second Nd:YAG laser cleaning with traditional mechanical and chemical methods. Stud Conserv. 2015;60:S58–64. https://doi.org/10.1179/0039363015Z.000000000208.

68. Nguyen TL, Saleh MA. Thermal degradation of azobenzene dyes. Results Chem. 2020;2:100085–7.

69. Qiu S, Chu H, Zou Y, Xiang C, Zhang H, Sun L, Xu F. Thermochemical studies of Rhodamine B and Rhodamine 6G by modulated differential scanning calorimetry and thermogravimetric analysis. J Therm Anal Calorim. 2016;123(2):1611–8.

Publisher's Note